Asia-Pacific Journal of Atmospheric Sciences
https://doi.org/10.1007/s13143-018-00099-1

Online ISSN 1976-7951
Print ISSN 1976-7633

ORIGINAL ARTICLE

Chemical Characteristics of Size-Resolved Aerosols in Coastal Areas during KORUS-AQ Campaign; Comparison of Ion Neutralization Model

Min-Suk Bae[1] · Taehyoung Lee[2] · James J. Schauer[3] · Gyutae Park[2] · Young-Baek Son[4] · Ki-Hyun Kim[5] · Seung-Sik Cho[6] · Seung Shik Park[7] · Kihong Park[8] · Zang-Ho Shon[9]

Received: 18 September 2018 / Revised: 25 November 2018 / Accepted: 8 December 2018

Abstract

Measurements for size-resolved chemical composition were made at the Anmyeon Island station on the western coast of the Republic of Korea between May 28 and June 20, 2016. This study determined the main chemical compositions of size-resolved particulate matter (i.e., organic carbon, elemental carbon, water-soluble organic carbon, water-soluble ions, and benzene carboxylic acids) from a total of eight chemically size-resolved sets using micro-orifice uniform deposit impactors. The sum of the species presents a prominent accumulation mode peak at a diameter of 0.56 μm without the coarse mode peak. In the accumulation mode, SO_4^{2-} (49.3%) was the dominant particle component in the size range of 0.1–1.8 μm. Organic carbon and elemental carbon accounted for 13.5% and 0.4%, respectively. Benzene carboxylic acids indicate the accumulation mode peak at the diameter of 0.56 μm. The size-resolved equivalent ion concentration ratios between all measured cations and anions and the ion neutralization model, which uses four major ions, were compared. As a result, the concentration of Na^+ is of importance in the accumulation mode for the equivalent ion concentration.

Keywords MOUDI · OPS · Benzene carboxylic acid · WSOC · OC

1 Introduction

Particulate matter (PM) has shown to be strongly associated with morbidity and mortality, so people around the world are taking it very seriously (Sahani et al. 2014; Huang et al. 2016; Maji et al. 2017; Tang et al. 2017). Toxicological studies have proven that ultrafine PM (i.e., $PM_{0.1}$) can penetrate deep into the alveoli of the lungs, resulting in adverse health effects (Liao et al. 2011; Salma et al. 2015). Size-resolved chemical compositions were investigated to assess the adverse health effects of PM, since size-resolved PM analyses are useful particularly to examine their properties across a wide range

Responsible Editor: Soon-Il An.

Electronic supplementary material The online version of this article (https://doi.org/10.1007/s13143-018-00099-1) contains supplementary material, which is available to authorized users.

✉ Min-Suk Bae
minsbae@mokpo.ac.kr

[1] Department of Environmental Engineering, Mokpo National University, Muan 58554, Republic of Korea

[2] Department of Environmental Science, Hankuk University of Foreign Studies, Gyeonggi 17035, Republic of Korea

[3] Department of Civil & Environmental Engineering, University of Wisconsin-Madison, Madison 53705, USA

[4] Korea Institute of Ocean Science & Technology, Jeju 63349, Republic of Korea

[5] Department of Civil and Environmental Engineering, Hanyang University, Seoul 04763, Republic of Korea

[6] Department of Pharmacy, College of Pharmacy, Mokpo National University, Muan 58554, Republic of Korea

[7] Department of Environment and Energy Engineering, Chonnam National University, Gwangju 61186, Republic of Korea

[8] School of Earth Sciences and Environmental Science and Engineering, Gwangju Institute of Science and Technology, Gwangju 61005, Republic of Korea

[9] Department of Environmental Engineering, Dong-Eui University, Busan 47340, Republic of Korea

Published online: 18 December 2018

of sizes as well as their associated impacts on the environment and on public health (e.g., interaction with climate variables, impact on the respiratory system upon inhalation, and long range transport) (Wang et al. 2011; Bae and Park 2013; Degrendele et al. 2016; Gong et al. 2016; Wu et al. 2017; Li et al. 2017). Although the results of studies have occasionally reported possible occurrences of negative artifacts, such as a significant evaporation loss of labile species at a low pressure (Zhang and McMurry 1992), and sulfates can also interact with the substrate (Kim et al. 2010), micro-orifice uniform deposit impactors (MOUDI) have been extensively used to collect PM to analyze the size-resolved chemical compositions (Ham and Kleeman 2011; Plaza et al. 2011; Park et al. 2013). In general, most mass fractions of water-soluble inorganic ions (e.g., nitrate, ammonium, or sulfate) at the coast or island were found in the coarse mode (> 1 μm) under clean marine conditions, while those found in the fine mode (< 1 μm) occurred during polluted flow conditions (Yeatman et al. 2001; Cavalli et al. 2004). In particular, high spatial variability across many elemental constituents was observed at the coastal site with diameters of 0.25–2.5 μm or less than 0.25 μm, and this trend was associated with motor vehicle use (Krudysz et al. 2008). The behavior of organic aerosols is affected by marine emissions of biogenic volatile organic compounds and primary organic aerosols (Gantt et al. 2010), and their distribution in the marine boundary layer or at the coast is strongly associated with seasonal patterns in ocean biology (O'Dowd et al. 2004). Products of organic carbon (OC) and elemental carbon (EC) concentrations at the marine boundary layer of the eastern Mediterranean were found in the fine mode while being water-soluble to a great extent (70%) (Bougiatioti et al. 2013). Products of secondary organic aerosol (SOA) from aromatic VOCs have been used as anthropogenic SOA tracers in identifying aerosol sources and source apportionment (Al-Naiema and Stone 2017). For instance, organic compounds besides poly aromatic hydrocarbons (PAHs) detected in the ultrafine size fraction of rice straw and benz[de]anthracen-7-one and 4-methylphenylacetone were found in cigarette smoke (Kleeman et al. 2008). Aromatic acids (e.g., benzoic acid (BA) and salicylic acids) have been shown to exist in urban particulate matter (Ho et al. 2011). BA emissions are primarily from various anthropogenic sources (i.e., automobile fumes, heavy-duty diesel trucks, and industrial boilers burning oil as fuel) (Rogge et al. 1997). The primary photodegradation products of petroleum hydrocarbons are benzene carboxylic acids (BCAs) with significant levels of BA that presumably form from the decomposition of alkyl-substituted benzenes. In a recent study, phthalic acid was also proposed as a tracer for the photooxidation of primary aromatic hydrocarbons (i.e., naphthalene and methylnaphthalenes) in $PM_{2.5}$ (Kawamura and Kaplan 1987; Kautzman et al. 2010; Kleindienst et al. 2012).

Ion balance analysis has been commonly used to understand atmospheric neutralization conditions. The molecular weight and mass concentrations of water-soluble ionic species are utilized to calculate corresponding microequivalent (μeq) ion concentrations. Generally, the size-resolved ionic balances have been investigated using only major cations and anions from time integrated PM samples or real time measurement (Zhang et al. 2007). However, particulates are external mixtures that are potentially quite close to neutral. Alkaline sea-salt and mineral particles, and possibly some organic acids of unknown ionic composition, were not well studied for ion balance associations. Prior studies have discussed the ion neutralizaiton method, which is used to infer the aerosol hydrogen ion loading, presented no agreement with aerosol pH predicted by multiple independent metrics (Guo et al. 2015; Hennigan et al. 2015).

The KORea-US Air Quality (KORUS-AQ) was planned to provide an opportunity to answer questions related to aerosol physical, optical, and chemical properties regarding the evolution of gas and aerosol phase reactivity in the unique East Asian environment. As a part of KORUS-AQ campaign, this study aimed to assess the size-resolved chemical compositions of aerosol particles (i.e., organic carbon (OC), water-soluble organic carbon (WSOC), elemental carbon (EC), water-soluble ions (WSI), and BCA) on the western coast of Korea. To accomplish this goal, we address the size-resolved chemical properties in the region, discuss different ionic balance approaches, and compare optical and chemical size distributions as well.

2 Experimental Methods

2.1 Sampling Site and Size-Resolved PM Sampling

Size-resolved PM sampling and measurements were carried out at Anmyeon Island in South Korea from May 28 to June 20, 2016. The sampling site is a Global Atmosphere Watch (GAW) Station managed by the World Meteorological Organization (WMO) in Korea. Anmyeon (36° 32' N, 126° 190′ E; 46 m above sea level (ASL)) station has been operating as a clean background (i.e., the western coast of Korea) to monitor the PM and gaseous components since 2003 (supplemental Fig. S1). The site receives both marine and continental air masses by local circulation, and the regional and long-range transport processes depend on the prevailing meteorological conditions (Kim et al. 2012; Shim et al. 2013; Jeon et al. 2015).

The filter-based 24-h (hr) integrated sampler was operated at the GAW. All samples used for each of the analyses were collected downstream of the $PM_{2.5}$ impactor (BMI Inc., USA) operating at a flow rate of 16.7 l per minute (lpm). The integrated samplers were equipped with a timer to allow the

sampler to start and stop at pre-programmed times. The 24-h integrated sampler was equipped with two sample trains downstream of the impactor. One train consisted of a single 47-mm Teflon filter (PTFE, R2PJ047, Pall Corp., USA) and the other train consisted of an organic denuder (Sunset Laboratory Inc., USA) followed by a 47-mm quartz fiber filter (Pallflex, 2500QATUP, Pall Corp., USA) both operated at 8.35 lpm. OC, EC, WSOC, and WSI were analyzed from samples collected on a quartz filter. Air flows through the integrated samplers were controlled using critical orifices for each train and were checked using a dry gas calibrator (Defender 510, Mesa Labs, Inc., USA) before and after each sampling. The organic denuder was fabricated with replaceable parallel charcoal-impregnated filter strips to collect gas-phase organic compounds (Mader et al. 2003). The organic denuder strips were changed at every 6th day.

$PM_{2.5}$ mass concentration (i.e., average of three analyses) was determined from the Teflon filter, which was weighed with a microbalance (DM, Sartorius Corp., Germany). Prior to weighing, the filters were conditioned for 24 h in a clean, controlled chamber (relative humidity less than 40% and temperature of approximately 20 °C). Size-resolved PM sampling was conducted using a MOUDI (MSP Corp., USA) with integrated sampling between 48 and 72 h. During the sampling periods, a total of eight sets were collected. The samples were collected using aerodynamic cutpoint diameters of 0.056, 0.1, 0.18, 0.32, 0.56, 1.0, 1.8, 3.2, 5.6, 10.0, and 18.0 μm on quartz filters (Pallflex, 2500QATUP, Pall Corp., USA). Thick-washers, which are commercially available (MSP Corp., USA), were installed between the stages on the MOUDI for quartz filter sampling. Due to analytical difficulty resulting from the small diameter (i.e., 25 mm) and amount of mass, filters with a diameter of 0.056 μm were not applied in this study. An inorganic annular denuder was not equipped for MOUDI system due to low removal efficiency at high flow rate (i.e., 30 lpm). Each filter was carefully cut into a certain amount of sampling-dotted areas using a 1.0 cm^2 punch for OC and EC analysis, so the remaining portions were extracted for WSOC, WSI, and BCA analysis. The detailed analytical methods can be found in prior publications (Bae and Park 2013; Park et al. 2013).

2.2 Size-Resolved Chemical Analysis

Carbonaceous analyses were performed using a thermal-optical transmittance carbon analyzer (Sunset Laboratory Inc., USA) (Bae et al. 2004a, b). The average of analytical recovery was 1.00 ± 0.02. Both the instrument blank test, which was conducted by completing the analysis without collecting aerosols, and the field blank test without collecting aerosols were performed to determine the noise and contamination. Duplication analysis for PM samples was performed for every five samples. To determine the water soluble species (i.e., WSOC and WSI), the remaining portions of the samples after OC and EC analyses were extracted. The detailed analytical procedures can be found in the previous publication (Bae et al., 2017).

To determine the WSOC and WSI species, the remaining portions of the samples after OC and EC analyses were extracted. The filter extraction process involved placing the filter in previously baked Pyrex glass vials containing 20 mL of milli-Q water each, then placing the vials in an ultrasonic bath at 20 °C controlled using a low temperature circulator (EYELA, Tokyo Rikakikai Co., Japan) for 120 min. All water extracts were filtered using a 0.45 μm membrane filter (Hydrophilic PTFE 0.45 μm pore size, Advantec, Japan) and were then analyzed for sodium (Na^+), ammonium (NH_4^+), potassium (K^+), calcium (Ca^{2+}), magnesium (Mg^{2+}), chloride (Cl^-), nitrate (NO_3^-), and sulfate (SO_4^{2-}) using ion chromatography (Metrohm 883, Switzerland). Metrohm Metrosep A Supp-5 with eluent of 3.2 mM Na_2CO_3 & 1.0 mM $NaHCO_3$ and Metrohm Metrosep C4–250 columns with 1.7 mM HNO_3 & 0.7 mM dipicolinic acid were used to analyze the anion and cation compounds, respectively. The injection volume was of 250 μl, and the method detection limit (MDL) was determined as 3.14 (i.e., pi) times the standard deviation of the lowest detected standard concentrations. The determined MDLs for Na^+, NH_4^+, K^+, Ca^{2+}, Mg^{2+}, Cl^-, NO_3^-, and SO_4^{2-} were 2, < 1.0, 3, 10, 11, 3, < 1.0, and < 1.0 ppb, respectively. The sample precision was less than 3.0% for all ionic compounds.

The remaining portion of the water extracts were analyzed using the TOC analyzer (Sievers 900, GE, USA) for WSOC. The TOC analyzer measures the organic carbon content by subtracting the measured carbon content of the two channels, which are the total carbon channel with ammonium persulfate and ultraviolet light and the inorganic carbon channel without ultraviolet light. The conductivity of water extracts through a semi-permeable membrane was measured. However, the inorganic carbon concentration causes higher analytical uncertainties, so an inorganic carbon remover (ICR) was installed to reduce the interference of inorganic carbon for the WSOC concentrations. The external sucrose standard was analyzed for quantification, and the average recovery was 1.00 ± 0.03.

An optical particle sizer (OPS, Model 3330, TSI Inc., USA) was deployed with a heating inlet to remove the moisture. The OPS measures the particle concentrations in a maximum of 16 size channels and detects scattered laser-light at a mean scattering angle of 90° with a parabolic mirror. With high time resolution and easy operability, it has been extensively used to determine the size-resolved number with converted mass concentrations (Zhao and Stephens 2017). However, the ratio of volume to mass (i.e., density) was required to calculate the size-resolved PM mass concentrations.

In this study, we compare 24-h integrated PM mass using the Teflon gravity method and volume concentrations to determine the real-time size-resolved PM mass concentrations from OPS. In this study, the PM samples were collected in the 12 ranges from 0.3 through 10 μm.

2.3 Underivatized Benzene Carboxylic Acids (BCAs)

An analysis of underivatized BCA is challenging due to the difficulty in its separation as well as the detection of these small polar analytes. In general, gas chromatography mass spectrometry (GCMS) has been widely used for BCA quantification, while an analytical technique requires extraction sequences using organic solvent and derivatization due to the analytical limitation for organic acids with heavy molecular weights (Rogge et al. 1997; Bae et al. 2014). In this study, the remaining extracts after analysis of the WSOC and WSI species were combined into a set of size-resolved PM extracts to analyze the underivatized BCAs using a liquid chromatography-tandem mass spectrometry (LC-MSMS). The composite extracts were completely dried using a freezing dryer (il-Shin Bio Base, South Korea) after an internal standard injection of phthalic acid - D4 (quantifier ion; 169.0 m/z). Hydrophilic interaction LC was carried out using an Eclipse XDB-C18 4.6 mm ID × 150 mm (5 μm) column as stationary phase with 10 mM ammonium acetate and acetonitrile in milli-Q water. It was combined with double MS in the multiple reaction monitoring (MRM) mode for the separation and detection of five underivatized BCAs (i.e., phthalic acid (1,2-BCA, quantifier ion; 165.1 m/z), terephtalic acid (1,4-BCA, 164.8 m/z), trimellitic acid (1,2,4-BCA, 165.2 m/z), trimesic acid (1,3,5-BCA, 209.1 m/z), and pyromellitic acid (1,2,4,5-BCA, 165.0 m/z)). Regression coefficients to determine the seven point calibrations varied from 0.998 to 0.999. Absolute MDLs (i.e., converted atmospheric concentration) were in the range of 1.72–4.61 pg/m^3. A fast screening method totaling 8 min of runtime was developed for use with samples characterized using very low analyte concentrations and complex matrices. The best analytical conditions in LC/MSMS and the final mass fragment transitions for quantification (i.e., quantifier and qualifier ions) are shown in supplemental Tables S1 and S2.

2.4 Ion Neutralization Model (INM)

The stoichiometric neutralization for the water-soluble ionic particles was obtained from a normalized ratio of the measured NH_4^+ (in nmol m^{-3}) to the neutralized NH_4^+ concentration (Zhang et al. 2007). The ion neutralization model (INM) has been frequently utilized to determine the acidic or neutral state of $PM_{1.0}$. The INM uses Eq. (1) to calculate the PM neutralization condition,

$$NH_4^+ \text{ measured}/NH_4^+ \text{ neutralized} = [NH_4^+/18]/[2 \times SO_4^{2-}/96 + NO_3^-/62 + Cl^-/35.5] \quad (1)$$

Numerous studies have been previously published using simple slope estimations between the value of [NH_4^+ measured] and [NH_4^+ neutralized] (Zhang et al. 2007; Han et al. 2016; Tan et al. 2016).

3 Results and Discussion

3.1 Size-Resolved Chemical Properties

The measurements were analyzed over different sampling times (i.e., 24-h integrated $PM_{2.5}$ mass using Teflon filter gravity method, 15-min $PM_{2.5}$ volume using OPS, and 48-h to 72-h integrated size-resolved PM using MOUDI). Fig. 1 presents complete time series traces for particle mass concentrations indicated with selected periods (1–4) based on MOUDI sampling periods. The four periods (1–4) were assessed from high concentration ranges. The selected periods are June 1–June 3, June 3–June 6, June 6–June 16, and June 16–June 19 named for period 1, period 2, period 3, and period 4, respectively. The amount of data available for each measurement allows for the initial validation, and data was flagged and removed from the analysis if certain conditions were known to apply: when less than 80% of the data was available for an hour; when an instrument was malfunctioning or under maintenance.

Figure 1a provides an overview of the temporal mass concentrations by the OPS in the size range from 0.3–2.5 μm. To present time and size-resolved PM mass concentrations from OPS, a slope of 2.01 ($R^2 = 0.71$) was applied to the size-resolved mass concentrations. A slope was determined by the relationship between daily-averaged $PM_{2.5}$ volume (vol.) concentrations using OPS (summed over the size range of 0.3–2.5 μm) and 24-h integrated $PM_{2.5}$ $mass_T$, which was measured using the Teflon gravity method. A pairwise correlation scatterplot (slope of 1.01 ± 0.148 (± standard error)) between daily averaged $PM_{2.5}$ $mass_P$, which was converted from $PM_{2.5}$ vol. and 24-h integrated $PM_{2.5}$ $mass_T$, is shown in supplemental Fig. S2(a). The characteristic feature of the data sets does not present a strong daily diurnal pattern, which implies that the sampling sites were not affected by strong local sources. The higher particle concentration events can be associated with regional and/or middle range transport, and the size range of 0.3–0.5 μm accounts for about 41.8% of the total mass concentrations in the size range of 0.3–

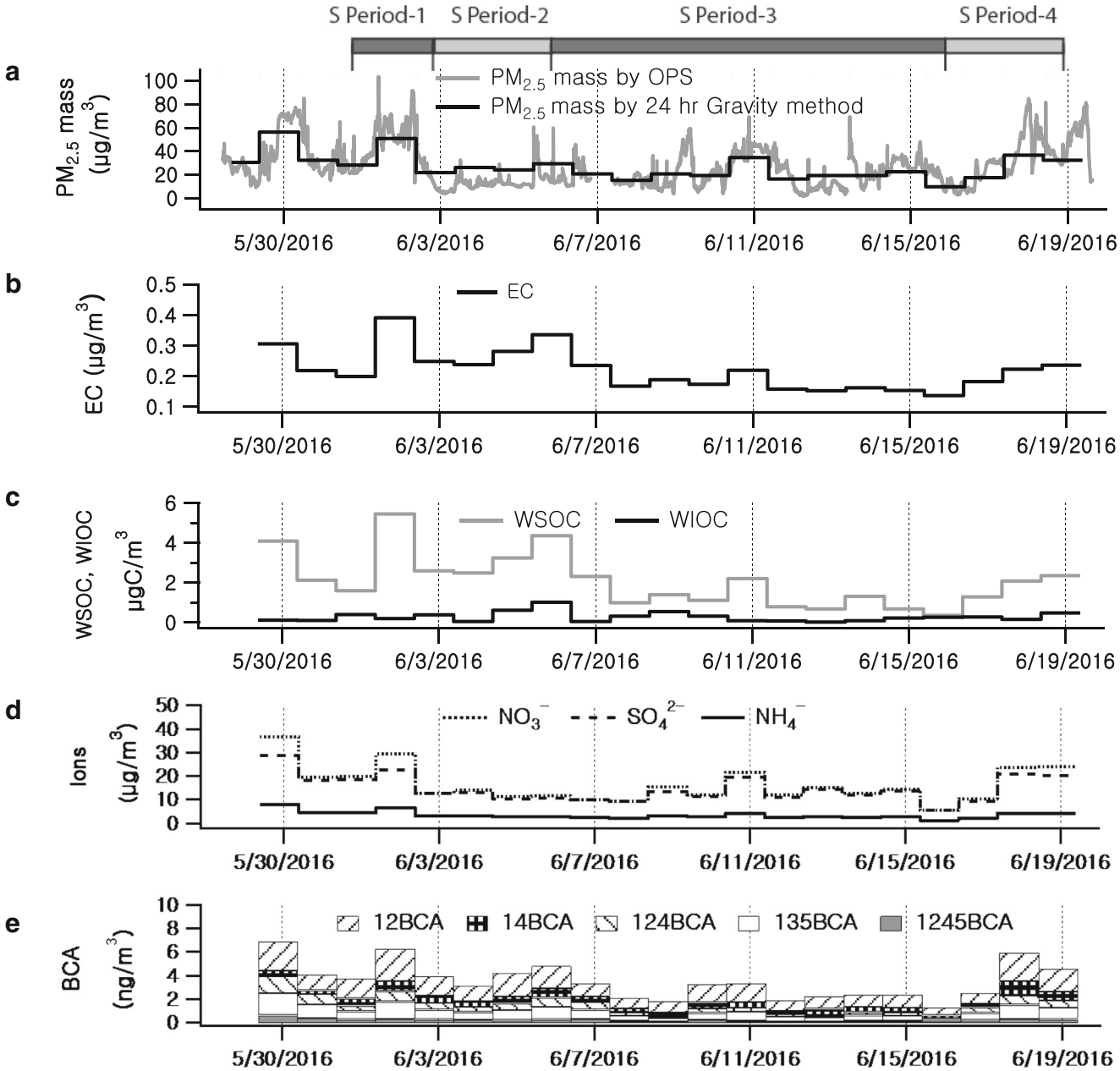

Fig. 1 **a** Time series of $PM_{2.5}$ $mass_T$ using Teflon filter gravity method and $PM_{2.5}$ $mass_P$ using optical particle size (OPS). **b** Time series of elemental carbon (EC). **c** Time series of water-soluble organic carbon (WSOC) and water-insoluble organic carbon (WIOC). **d** Time series of NO_3^-, SO_4^{2-}, and NH_4^+. **e** Time series of underivatized phthalic acid (1,2-BCA), terephtalic acid (1,4-BCA), trimellitic acid (1,2,4-BCA), trimesic acid (1,3,5-BCA), and pyromellitic acid (1,2,4,5-BCA) in $PM_{2.5}$

10.0 μm. Table 1 shows the statistical results for the concentration during the sampling period. The average concentration of $PM_{2.5}$ $mass_T$, $PM_{2.5}$ volume, and $PM_{2.5}$ $mass_P$ are 24.3 ± 2.3 μg/m^3 (average ± standard error), 12.3 ± 1.6 nL/m^3, and 24.8 ± 3.3 μg/m^3, respectively. The overall concentrations of $PM_{2.5}$ $mass_T$ and $PM_{2.5}$ $mass_P$ are statistically indistinguishable with a 95% confidence level.

Table S3 of the supplemental material presents the size distribution (i.e., 10 different aerodynamic cutpoint diameters using MOUDI) of all species for size-resolved OC, EC, WSOC, and WSI concentrations. A previous size-resolved PM study (Xu et al. 2016) showed that organic aerosol (OA) accounts for 51%, followed by NO_3^- (17%), SO_4^{2-} (13%), NH_4^+ (10%), BC (6%), and Cl^- (3%), which peaked at about 0.5 μm for the wintertime in a highly polluted city of China. Xu et al. (2015) found less OA fraction in an unpolluted area, such as a remote high-altitude (4180 m) location in the northeastern part of the Tibetan Plateau, China (e.g., SO_4^{2-} (36%), OC (18%), NO_3^- (17%), NH_4^+ (10%), Ca^{2+} (6.6%), and EC (2.6%) in $PM_{2.5}$ for summertime). However, the size distributions of chemical components were different. The size distributions of SO_4^{2-} and NH_4^+ peaked in the accumulation mode

Table 1 Statistical results of the concentration of $PM_{2.5}$ $mass_T$, $PM_{2.5}$ volume, and $PM_{2.5}$ $mass_P$ for the sampling period

	Average	Median	Standard Deviation	Minimum	Maximum
$PM_{2.5}$ $mass_T$ [a]	24.31	21.29	9.58	9.80	50.71
$PM_{2.5}$ vol. [b]	12.30	10.15	6.88	4.71	29.37
$PM_{2.5}$ $mass_P$ [c]	24.75	20.43	13.85	9.48	59.13

[a] 24-h integrated $PM_{2.5}$ mass concentration using Teflon filter gravity method (unit: $\mu g/m^3$)

[b] Daily averaged $PM_{2.5}$ volume concentration using optical particle sizer (OPS, Σ dp 0.3–2.5 μm) (unit: nL/m^3)

[c] Daily averaged $PM_{2.5}$ mass concentration using optical particle sizer (OPS, Σ dp 0.3–2.5 μm) (unit: $\mu g/m^3$)

(0.32–0.56 μm), while those of both NO_3^- and Ca^{2+} peaked in the range of 1.8–3.2 μm (Xu et al. 2015). In this study, the sum of species presents a prominent accumulation mode peak at a diameter of 0.56 μm without the coarse mode peak. In the accumulation mode, SO_4^{2-} (49.3%) dominated over the composition of particles in the size range of 0.1–1.8 μm, followed by NH_4^+ (19.5%) and NO_3^- (13.6%). The OC and EC account for 13.5% and 0.4%, respectively. However, OC (37.5%) dominates at diameters smaller than 0.18 μm, with SO_4^{2-} contributing 29.6%. In the coarse mode, NO_3^-, the main contributor, accounts for 34.0% of the particle mass in the size range of 3.2–18.0 μm, followed by SO_4^{2-} (16%), OC (15%), NH_4^+ (5%), and the rest of the species in total accounted for 64% in this size range. The species that are relatively abundant in the accumulation mode aerosols are mainly secondary species, including NH_4^+, SO_4^{2-}, and OC, while the species that are relatively abundant in the coarse mode aerosols could mainly be primary mineral ionic species such as Ca^{2+}, Na^+, and Cl^-. NO_3^- is also closely associated with dust particles as a result of its formation through the reactions of HNO_3 gas with carbonate salts (e.g., calcite and dolomite) (Sullivan et al. 2009) which could form $Ca(NO_3)_2$ and $Mg(NO_3)_2$ (Li and Shao 2009).

To investigate the size-resolved chemical characteristics for the selected periods, the average size distributions of the mass concentrations of WSOC, water insoluble organic carbon (WIOC) (i.e., differences between OC and WSOC), EC, and WSIs and ($Na^+ + Cl^-$) to ($WSOC + NH_4^+ + NO_3^- + SO_4^{2-}$) in different size bins are shown in Figs. 2 and 3, which can provide information on the marine origin. The results statistical for the concentration of the selected sampling periods 1–4 are presented in Table 2. The relative fractional contributions of the individual species in different size bins are shown in Supplemental Fig. S3 as well.

For period 1, the high $PM_{2.5}$ mass (36.3 ± 20.4 $\mu g/m^3$) (average ± standard deviation), OC (4.03 ± 2.02 $\mu g/m^3$), and BCAs (5.12 ± 1.65 ng/m^3) were analyzed in comparison to the other periods. The sum of the species presents a prominent accumulation mode peak at a diameter of 0.56 μm without a clear coarse mode peak. WSOC (28%) dominates the composition of the particles at a diameter of 0.1 μm in the accumulation mode and then gradually decreases into the coarse mode. The average mass fraction in the accumulation mode in the size range of 0.1–1.8 μm is 17%, while this fraction in the coarse mode of the size range of 3.2–18.0 μm is 10%. WIOC accounts for 8.4% and 8.5% in the accumulation mode and coarse mode, respectively, and shows no clear statistically significant differences between the accumulation and coarse mode. EC (1.3%) dominates in the size range of 3.2–18.0 μm in the coarse mode rather than in the accumulation mode (0.69%). SO_4^{2-} (40.6%) and NH_4^+ (16.2%) in the accumulation mode present the most dominant components in the PM while NO_3^- (38%) in the coarse mode shows the most dominant component in the PM. This suggests different secondary inorganic aerosol formation pathways between NO_3^- and SO_4^{2-}, supporting the possibility of nitrate aerosol formation through a reaction of the precursor (HNO_3) with the carbonate salts in the coarse mode (Sullivan et al. 2009). SO_4^{2-} (15%) and NH_4^+ (4%) in the coarse mode showed a relatively smaller fraction in the PM compared to the accumulation mode. Cl^- and Na^+ clearly dominate, accounting for 2.3% and 10.9% in the coarse mode of the size range from 3.2–18.0 μm, respectively, implying a marine source. In addition, K^+, Ca^{2+}, and Mg^{2+} dominate in the coarse mode, accounting for 1.2%, 1.1%, and 6.9%, respectively.

Unlike period 1, the sum of the species for period 2 shows a bimodal distribution at two modes: an accumulation mode peak at a diameter of 0.56 μm and the coarse mode peak at a diameter of 3.2 μm. Higher concentrations of NO_3^-, WIOC, and EC lead to a clear distribution in the coarse mode. Both WSOC (16%) and WIOC (11%) dominate in the accumulation mode. EC (2.7%) is predominantly in the coarse mode of the size range of 3.2–18.0 μm rather than in the accumulation mode (1.1%). Stone et al. (2011) argued that carbonaceous aerosol (OC and EC) that are typically found in fine particles can be included in coarse particles during a dust event, being internally mixed with dust (Stone et al. 2011). Therefore, EC prevalence in the coarse mode rather than in the accumulation mode might be due in large part to dust source contributions. SO_4^{2-} (31%) and NH_4^+ (15%) in the accumulation mode present the most dominant components.

For period 3, the relatively low $PM_{2.5}$ mass (19.8 ± 6.3 $\mu g/m^3$), OC (1.1 ± 0.6 $\mu g/m^3$), and BCAs ($2.4 \pm$

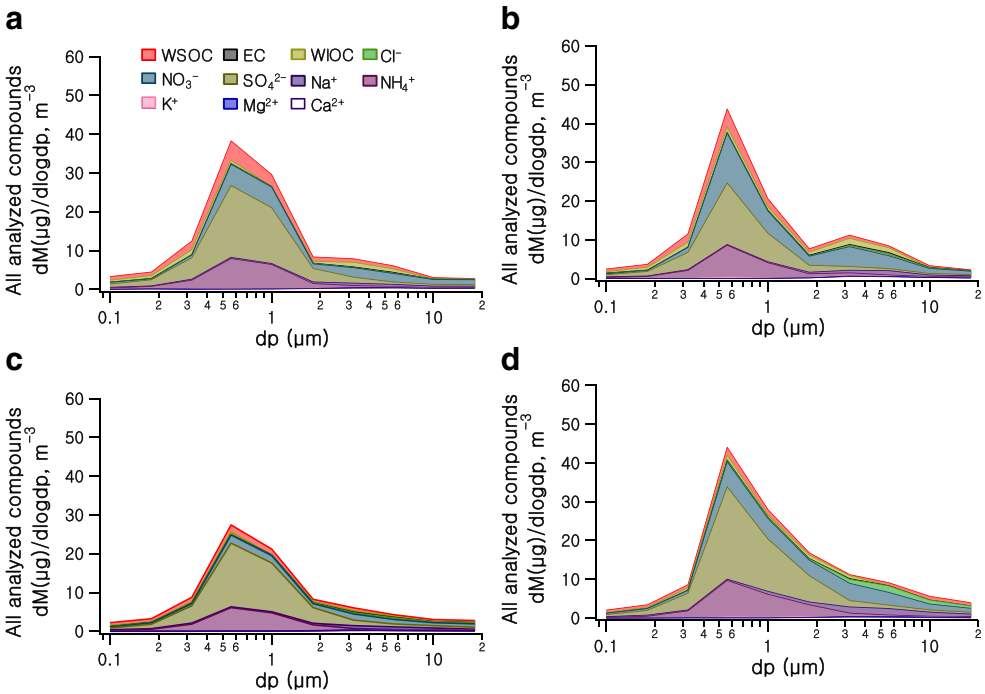

Fig. 2 Average size distributions for the mass concentrations of WSOC, WIOC, EC, and WSIs for the selected period 1(**a**), 2(**b**), 3(**c**), and 4(**d**)

0.7 ng/m^3) were analyzed (Table 2). The sum of the species presents a prominent accumulation mode peak at a diameter of 0.56 μm without the coarse mode as well. WSOC (15%) dominates the composition of the particles both in the accumulation mode and in the coarse mode.

For period 4, WSOC (12%) dominates over the composition of particles both on the accumulation mode and in the coarse mode. WIOC accounts for 5.2% and 1.7% in the accumulation mode and in the coarse mode, respectively. The size-resolved ratios of $Na^+ + Cl^-$ to $WSOC + NH_4^+ + NO_3^- + SO_4^{2-}$

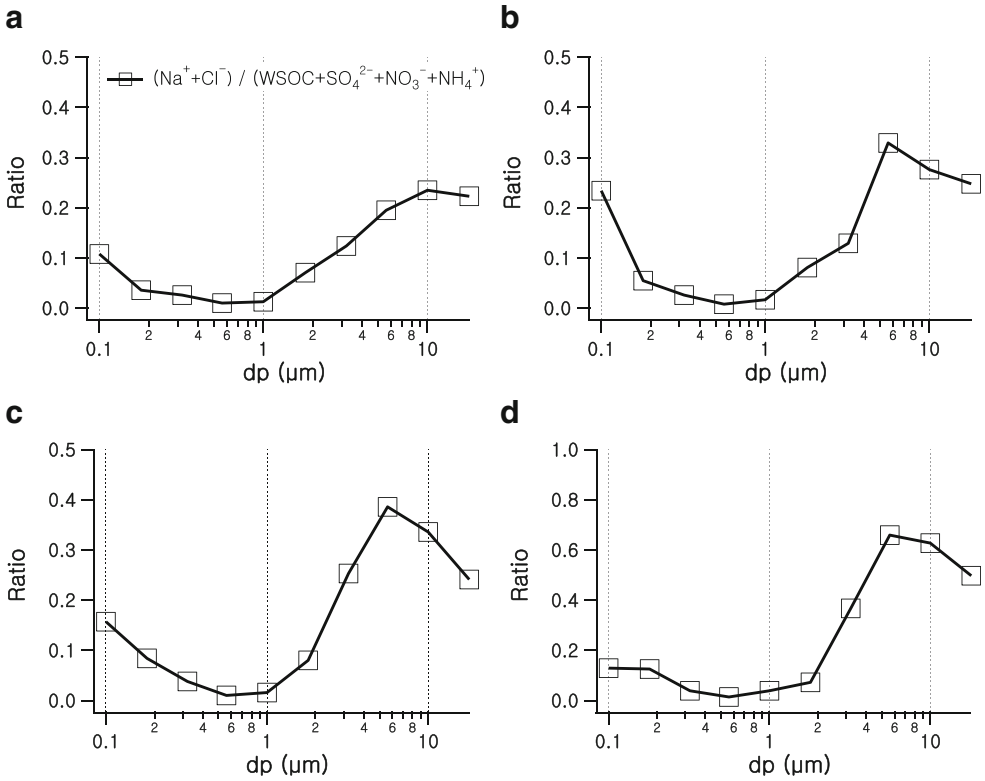

Fig. 3 The ratios of $Na^+ + Cl^-$ to $WSOC + NH_4^+ + NO_3^- + SO_4^{2-}$ in different size bins for the selected period 1(**a**), 2(**b**), 3(**c**), and 4(**d**)

Table 2 Statistical concentration results for the selected sampling periods 1–4

	Period 1 [a]	Period 2	Period 3	Period 4
$PM_{2.5}$ $mass_T$ ($\mu g/m^3$) [b]	36.29 ± 20.40	26.68 ± 2.66	19.83 ± 6.34	28.89 ± 9.99
OC ($\mu g/m^3$)	4.03 ± 2.02	3.33 ± 0.99	1.12 ± 0.62	1.91 ± 0.55
EC ($\mu g/m^3$)	0.32 ± 0.10	0.29 ± 0.05	0.18 ± 0.03	0.21 ± 0.03
EC/OC	0.08 ± 0.02	0.09 ± 0.01	0.19 ± 0.08	0.12 ± 0.02
WSOC/OC	0.91 ± 0.08	0.87 ± 0.14	0.82 ± 0.31	0.83 ± 0.08
WSOC ($\mu g/m^3$)	3.73 ± 2.15	2.80 ± 0.47	0.98 ± 0.70	1.60 ± 0.51
Total anions ($\mu g/m^3$) [c]	16.24 ± 9.26	9.51 ± 1.13	10.11 ± 3.58	15.87 ± 6.64
Total cations ($\mu g/m^3$) [d]	5.23 ± 2.58	3.30 ± 0.25	3.00 ± 0.81	3.90 ± 1.28
1,2-BCA (ng/m^3)	2.17 ± 0.78	1.73 ± 0.39	1.09 ± 0.29	1.76 ± 0.78
1,4-BCA (ng/m^3)	0.76 ± 0.18	0.62 0.15	0.39 ± 0.11	0.76 ± 0.45
1,2,4-BCA (ng/m^3)	0.74 ± 0.21	0.60 ± 0.15	0.29 ± 0.15	0.63 ± 0.16
1,3,5-BCA (ng/m^3)	1.16 ± 0.47	0.87 ± 0.21	0.48 ± 0.19	0.94 ± 0.31
1,2,4,5-BCA (ng/m^3)	0.30 ± 0.01	0.25 ± 0.03	0.17 ± 0.07	0.29 ± 0.05
BCA Sum (ng/m^3)	5.12 ± 1.65	4.07 ± 0.87	2.42 ± 0.70	4.37 ± 1.73

[a] Average ± standard deviation

[b] 24-h integrated $PM_{2.5}$ mass concentration using Teflon filter gravity method (unit: $\mu g/m^3$)

[c] Sum of Cl^-, NO_3^-, and SO_4^{2-}

[d] Sum of Na^+, NH_4^+, K^+, Ca^{2+}, and Mg^{2+}

$^-$ provide information on the marine origin. This indicates that, for these periods, the size-resolved chemical components were affected significantly by marine sources. Relative higher ratio in the smallest bin (i.e., 0.1 μm) can be relatively lower mass concentrations of sum of WSOC, NH_4^+, NO_3^-, and SO_4^{2-} with consistent concentrations of Na^+ in the accumulation mode (supplemental Fig. S1).

3.2 Investigation of Marine Sources

The secondary production and sea salt of Korea, including the Yellow Sea and eastern China, for periods 3 and 4 might have significantly affected the size distribution of the aerosol components. The size-resolved chemical characteristics of the marine sources with minimal anthropogenic source contribution were investigated. One MOUDI dataset (from June 13 to Jun 16 in period 3) was chosen by (1) eBC concentrations of less than 1.0 $\mu g/m^3$ using a Multi-Angle Absorption Photometer (MAAP) (Model 5012, Thermo Fisher Scientific Inc., USA) and (2) wind direction of the western marine side (225-315°). The time series of the eBC with selected conditions and the size distributions of the mass concentrations of OC, EC, and WSIs are shown in supplemental Fig. S4.

The concentration in the coarse mode showed a higher concentration than in the accumulation mode. Cl^- and Na^+ clearly dominate in the coarse mode, which confirms the marine source. In this period, low $PM_{2.5}$ mass (17.26 $\mu g/m^3$) and organic carbon (0.64 $\mu g/m^3$) were measured, and the higher ratio of WSOC to OC was 0.91. The marine-originated organic acids (e.g., hydroxy fatty acids, free amino acids, methanesulfonic acid, etc.) can result in an increase in the ratio of WSOC to OC (Kouvarakis and Mihalopoulos 2002; Mandalakis et al. 2011; Tyagi et al. 2015). Four-day averaged chlorophyll-a information using data from Geostationary Ocean Color Imager (GOCI) (i.e., launch on June 27, 2010 from South Korea with an hourly repeat cycle and 500 m spatial resolution) are shown in supplemental Fig. S5 (Ruddick et al. 2014). These images indicate that the OC concentration in the accumulation and coarse modes during the sampling periods (period 3) for the marine sector might be correlated with a relatively high chlorophyll-a concentration in the coastal area of the Yellow Sea, which could be one of the WSOC marine aerosol sources contributing to the sampling site.

3.3 Size-Resolved Benzene Carboxylic Acids

Furthermore, burning large amounts of coal and biomass in East Asia (e.g., eastern areas of China) adds more anthropogenic aerosols which alter the chemical composition of aerosols in the remote Yellow Sea atmosphere (Bae et al. 2014). Many organic compounds are photochemically oxidized, producing organic aerosol during long-range transport. Bae et al. (2014) showed that organic molecular markers (e.g., levoglucosan, PAHs, and BCAs) analyzed via GCMS were certainly influenced by the long-range transport of emissions from biomass burning on the Asian continent. Water-soluble diacids with low molecular weights have previously been studied (Deshmukh et al. 2016), whereas the size-resolved characteristics of BCAs have not been studied in the western North Pacific Rim. Although only one overall size distribution of BCAs

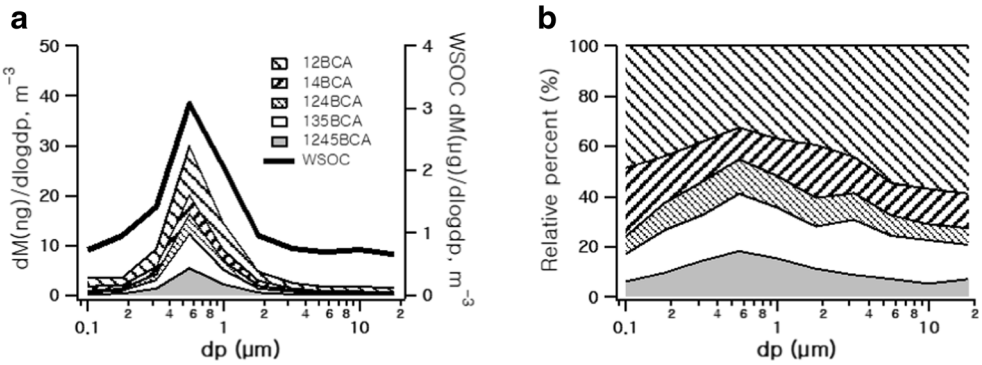

Fig. 4 **a** Average size distributions of the mass concentrations of benzene carboxylic acid and (**b**) the relative fractional contributions of individual species in different size bins for the entire sampling period

was displayed in this study due to the limited amount of sample composite extracts, as was discussed in the methods, this figure is reported for the first time. The sum of the BCAs indicates the accumulation mode peak at a diameter of 0.56 μm without the coarse mode, as shown in Fig. 4. 1,2-BCA accounts for the most abundance. 1,4-BCA was predominantly in the accumulation mode. Based on a good agreement ($R^2 = 0.98$) with size-resolved BCAs and WSOC, the size-resolved chemical characteristics of WSOC implies a common origin, and detailed examinations will be shown after further study.

3.4 Size-Resolved Equivalent Ion Concentration

Figure 5 shows pairwise scatterplots for four periods between μeq NH_4^+ and μeq SO_4^+ colored by logdp. Although the correlation of determinations (R^2) between μeq NH_4^+ and μeq SO_4^{2-} are 0.999, 0.998, 0.999, and 0.997 for periods 1–4, respectively, the slopes are statistically different. Incomplete neutralization can be due to the concurrent presence of other hydrogen-containing ionic compounds. Figure 6 shows size-resolved equivalent ion concentration ratios between all measured cations and anions, between measured cations without Na^+ and anions, and the INM using Eq. (1) for the selected periods (1–4) with uncertainties. The uncertainty was calculated using the error propagation method (Bae et al. 2006). On the basis of a theoretical definition, the aerosols appear to be neutralized by ionic balance for all size ranges. However, there were "more acidic" conditions observed by the INM for both the accumulation and coarse modes for all periods. However, the ratio calculated by the equivalent ion concentration using all measured cations and anions showed around unity, considering uncertainties over the accumulation mode and the coarse mode. This indicates that these particles are close to neutral or toward basic. It is very clear that the size-resolved equivalent ion concentration between measured cations without Na^+ and anions presents "more acidic" conditions than the INM for both the accumulation and coarse modes for all periods. Thus, the concentrations of Na^+ cannot be disregarded in the accumulation mode, which is the size range for the INM. In addition, the enhancement of the organic acid concentrations can also be attributed to the acid-catalyzed secondary organic aerosol formation. Therefore, many previous studies based on the INM could have higher uncertainties. Dicarboxylic acids in the ambient aerosols are the

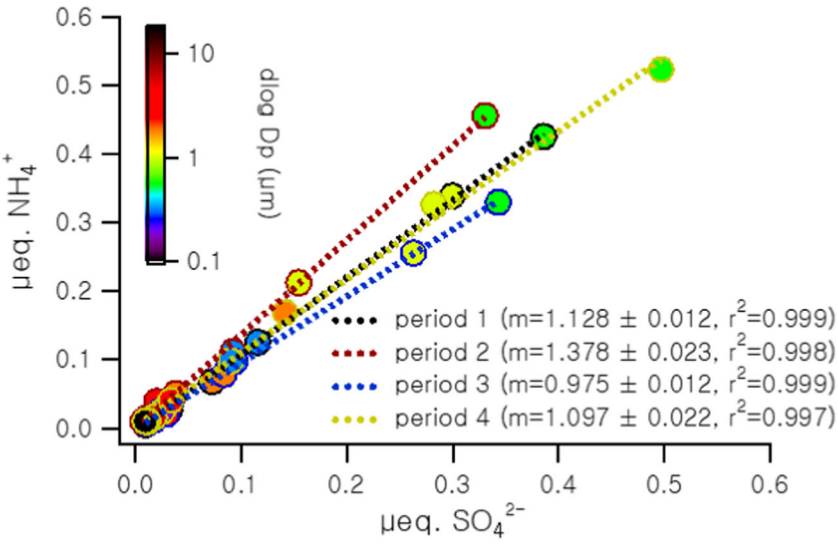

Fig. 5 Pairwise scatterplot between μeq NH_4^+ and μeq SO_4^+ for periods 1–4 colored by logdp

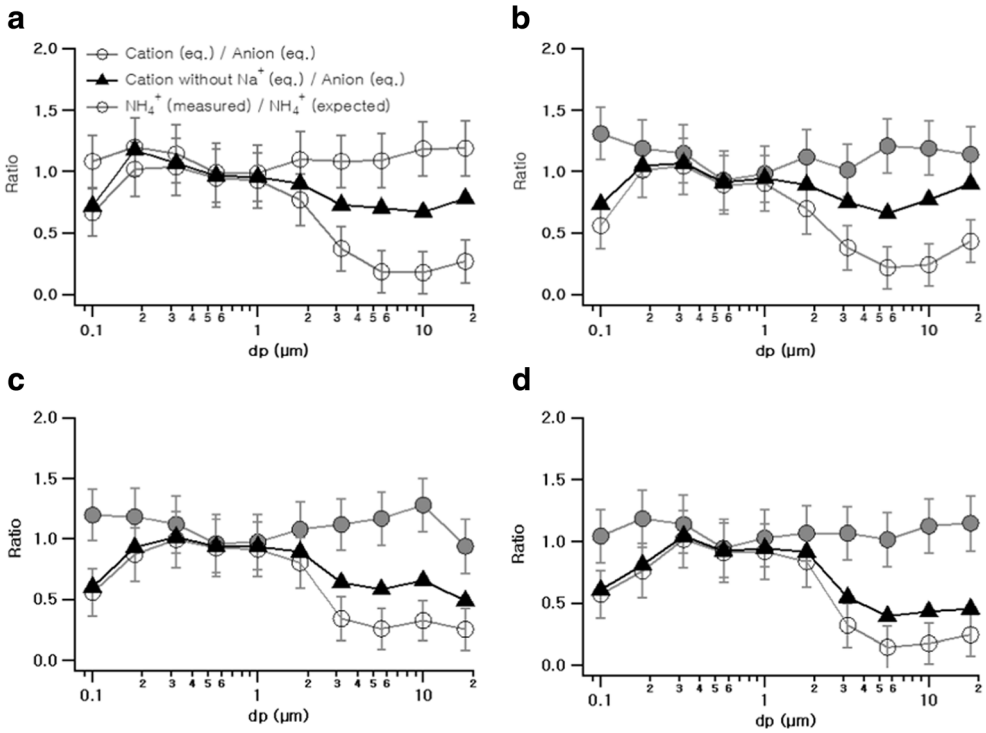

Fig. 6 Size-resolved ionic balance (with and without Na^+) in equivalent ion concentration and expected acidity for the selected period 1(**a**), 2(**b**), 3(**c**), and 4(**d**)

major compound class that significantly contribute to WSOC over the northwestern Pacific region (Simoneit et al. 2004). In this region, more organic acids can be expected since organic acids in WSOC originate from a variety of sources and are therefore more likely to be enriched than sea-salt particles. The very probable presence of organic acids, such as the BCAs in the submicron particles, indicates that these particles are expected to be more neutral. Therefore, the presence of high water-soluble organic carbon (e.g., BCAs) could deliver higher impacts to the ion equivalent ion concentration in the accumulation mode.

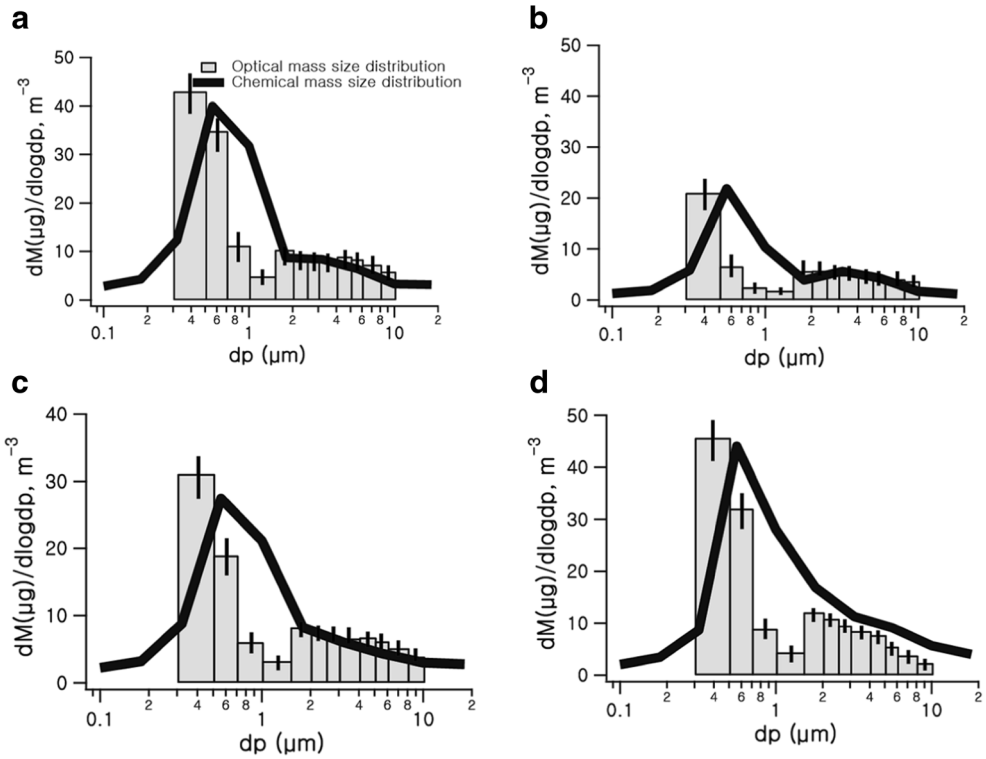

Fig. 7 Comparison between optical and chemical mass size distributions using OPS and MOUDI for the selected period 1(**a**), 2(**b**), 3(**d**), and 4(**d**)

3.5 Comparison of Optical and Chemical Size Distributions

Comparisons of the OPS to the MOUDI on the average size distributions of particle mass during the sampling periods are shown in Fig. 7. Our approach is based on the fact that agreement between OPS mass distributions, which are converted from the ratio of volume to mass as 2.01, is a convenient measurement of the mass concentrations. The average mass distributions obtained by the OPS and the MOUDI agree quite well for the coarse mode, but at the accumulation mode, the MOUDI shifts into larger size ranges when compared to OPS. Such a discrepancy was observed for all periods when comparing the OPS and MOUDI distributions because (1) the OPS only measured the scattering (e.g., EC measured by absorption); (2) responds differently to the particle shape as the particle becomes less spherical, which can increase the uncertainty; (3) the vacuum cutpoint diameter measured by MOUDI vs. the optical intensity diameter by OPS; and (4) limitation of understanding size resolved densities. The ratio of the organic mass (OM) to OC and unknown oxidized trace elements for MOUDI can be additional reasons. These possibilities lead to differences in the accumulation mode between the OPS and MOUDI. The four periods are consistent with respect to the differences between the concentrations of particle mass obtained via the OPS and MOUDI. In general, these two analyses fairly agree on the size distributions over the size ranges.

4 Conclusions

This study characterized the size-resolved main chemical compositions of aerosol particles (OC, WSOC, EC, WSI, and BCA) from a total of eight sets using MOUDI on the western coast of Korea during KORUS-AQ campaign. The sum of the species presents a prominent accumulation mode peak at a diameter of 0.56 μm, without the coarse mode peak. In the accumulation mode, SO_4^{2-} (49.29%) dominates the composition of the particles in the size range of 0.1–1.8 μm, followed by NH_4^+ (19.53%) and NO_3^- (13.64%). OC and EC account for 13.49% and 0.39%, respectively. 1,2-BCA dominates in the accumulation mode and in the coarse mode. The differences between the size-resolved equivalent ion concentration ratios and the ion neutralization model (INM) are related to the concentrations of Na^+, which cannot be disregarded in the accumulation mode. The enhancement of the organic acid concentrations can also be attributed for the neutrality. The reasons for the differences in the average size distributions of the particle mass using the OPS and the MOUDI measurements are that the OPS only measures scattering, the particle shape as the particle becomes less spherical, and the vacuum cutpoint diameter is measured by MOUDI. The information and knowledge collected in this study can be used to identify sources of aerosols of different sizes and/or to determine health effects.

Acknowledgements We acknowledge the support provided by the National Research Foundation of Korea (NRF) (NRF-2018R1A2A1A05077650 & 2017M3D8A1092222).

References

Al-Naiema, I.M., Stone, E.A.: Evaluation of anthropogenic secondary organic aerosol tracers from aromatic hydrocarbons. Atmos. Chem. Phys. **17**, 2053–2065 (2017)

Bae, M.S., Park, S.-S.: Thermal distribution of size-resolved carbonaceous aerosols and water soluble organic carbon in emissions from biomass burning. Asian J. Atmos. Environ. **7**, 95–104 (2013)

Bae, M.S., Schauer, J.J., DeMinter, J.T., Turner, J.R.: Hourly and daily patterns of particle-phase organic and elemental carbon concentrations in the urban atmosphere. J. Air Waste Manage. Assoc. **54**, 823–833 (2004a)

Bae, M.S., Schauer, J.J., DeMinter, J.T., Turner, J.R., Smith, D., Cary, R.A.: Validation of a semi-continuous instrument for elemental carbon and organic carbon using a thermal-optical method. Atmos. Environ. **38**, 2885–2893 (2004b)

Bae, M.S., Demerjian, K.L., Schwab, J.J.: Seasonal estimation of organic mass to organic carbon in PM2.5 at rural and urban locations in New York state. Atmos. Environ. **40**, 7467–7479 (2006)

Bae, M.S., Shin, J.S., Lee, K.Y., Lee, K.H., Kim, Y.J.: Long-range transport of biomass burning emissions based on organic molecular markers and carbonaceous thermal distribution. Sci. Total Environ. **466-467**, 56–66 (2014)

Bae, M.S., Schauer, J.J., Lee, T., Jeong, J.-H., Kim, Y.-K., Ro, C.-U., Song, S.-K.,, Shon, Z.-H.: Relationship between reactive oxygen species and water-soluble organic compounds: Time-resolved benzene carboxylic acids measurement in the coastal area during the KORUS-AQ campaign, Environ. Pollut. **231**, 1–12 (2017)

Bougiatioti, A., Zarmpas, P., Koulouri, E., Antoniou, M., Theodosi, C., Kouvarakis, G., Saarikoski, S., Mäkelä, T., Hillamo, R., Mihalopoulos, N.: Organic, elemental and water-soluble organic carbon in size segregated aerosols, in the marine boundary layer of the eastern Mediterranean. Atmos. Environ. **64**, 251–262 (2013)

Cavalli, F., Facchini, M.C., Decesari, S., Mircea, M., Emblico, L., Fuzzi, S., Ceburnis, D., Yoon, Y.J., O'Dowd, C.D., Putaud, J.P., Dell'Acqua, A.: Advances in characterization of size-resolved organic matter in marine aerosol over the North Atlantic. J. Geophys. Res. Atmos. **109**, D24215 (2004)

Degrendele, C., Okonski, K., Melymuk, L., Landlová, L., Kukučka, P., Audy, O., Kohoutek, J., Čupr, P., Klánová, J.: Pesticides in the atmosphere: a comparison of gas-particle partitioning and particle size distribution of legacy and current-use pesticides. Atmos. Chem. Phys. **16**, 1531–1544 (2016)

Deshmukh, D.K., Kawamura, K., Lazaar, M., Kunwar, B., Boreddy, S.K.R.: Dicarboxylic acids, oxoacids, benzoic acid, α-dicarbonyls, WSOC, OC, and ions in spring aerosols from Okinawa Island in the western North Pacific rim: size distributions and formation processes. Atmos. Chem. Phys. **16**, 5263–5282 (2016)

Gantt, B., Meskhidze, N., Carlton, A.G.: The contribution of marine organics to the air quality of the western United States. Atmos. Chem. Phys. **10**, 7415–7423 (2010)

Gong, X., Zhang, C., Chen, H., Nizkorodov, S.A., Chen, J., Yang, X.: Size distribution and mixing state of black carbon particles during a heavy air pollution episode in Shanghai. Atmos. Chem. Phys. **16**, 5399–5411 (2016)

Guo, H., Xu, L., Bougiatioti, A., Cerully, K.M., Capps, S.L., Hite Jr., J.R., Carlton, A.G., Lee, S.H., Bergin, M.H., Ng, N.L., Nenes, A., Weber, R.J.: Fine-particle water and pH in the southeastern United States. Atmos. Chem. Phys. **15**, 5211–5228 (2015)

Ham, W.A., Kleeman, M.J.: Size-resolved source apportionment of carbonaceous particulate matter in urban and rural sites in Central California. Atmos. Environ. **45**, 3988–3995 (2011)

Han, Y., Stroud, C.A., Liggio, J., Li, S.M.: The effect of particle acidity on secondary organic aerosol formation from α-pinene photooxidation under atmospherically relevant conditions. Atmos. Chem. Phys. **16**, 13929–13944 (2016)

Hennigan, C.J., Izumi, J., Sullivan, A.P., Weber, R.J.: Nenes, A. a critical evaluation of proxy methods used to estimate the acidity of atmospheric particles. Atmos. Chem. Phys. **15**, 2775–2790 (2015)

Ho, K.F., Ho, S.S., Lee, S.C., Kawamura, K., Zou, S.C., Cao, J.J., Xu, H.M.: Summer and winter variations of dicarboxylic acids, fatty acids and benzoic acid in $PM_{2.5}$ in Pearl Delta river region, China. Atmos. Chem. Phys. **11**, 2197–2208 (2011)

Huang, C.L., Bao, L.J., Luo, P., Wang, Z.Y., Li, S.M., Zeng, E.Y.: Potential health risk for residents around a typical e-waste recycling zone via inhalation of size-fractionated particle-bound heavy metals. J. Hazard. Mater. **317**, 449–456 (2016)

Jeon, W., Choi, Y., Lee, H.W., Lee, S.H., Yoo, J.W., Park, J., Lee, H.J.: A quantitative analysis of grid nudging effect on each process of PM2.5 production in the Korean peninsula. Atmos. Environ. **122**, 763–774 (2015)

Kautzman, K.E., Surratt, J.D., Chan, M.N., Chan, A.W.H., Hersey, S.P., Chhabra, P.S., Dalleska, N.F., Wennberg, P.O., Flagan, R.C., Seinfeld, J.H.: Chemical composition of gas- and aerosol-phase products from the Photooxidation of naphthalene. J. Phys. Chem. **114**, 913–934 (2010)

Kawamura, K., Kaplan, I.R.: Motor exhaust emissions as a primary source for dicarboxylic acids in Los Angeles ambient air. Environ. Sci. Technol. **21**, 105–110 (1987)

Kim, K.H., Sekiguchi, K., Kudo, S., Sakamoto, K., Hata, M., Furuuchi, M., Otani, Y., Tajima, N.: Performance test of an inertial fibrous filter for ultrafine particle collection and the possible sulfate loss when using an aluminum substrate with ultrasonic extraction of ionic compounds. Aerosol Air Qual. Res. **10**, 616–624 (2010)

Kim, W., Doh, S.J., Yu, Y.: Asian dust storm as conveyance media of anthropogenic pollutants. Atmos. Environ. **49**, 41–50 (2012)

Kleeman, M.J., Robert, M.A., Riddle, S.G., Fine, P.M., Hays, M.D., Schauer, J.J., Hannigan, M.P.: Size distribution of trace organic species emitted from biomass combustion and meat charbroiling. Atmos. Environ. **42**, 3059–3075 (2008)

Kleindienst, T.E., Jaoui, M., Lewandowski, M., Offenberg, J.M., Docherty, K.S.: The formation of SOA and chemical tracer compounds from the photooxidation of naphthalene and its methyl analogs in the presence and absence of nitrogen oxides. Atmos. Chem. Phys. **12**, 8711–8726 (2012)

Kouvarakis, G., Mihalopoulos, N.: Seasonal variation of dimethylsulfide in the gas phase and of methanesulfonate and non-sea-salt sulfate in the aerosols phase in the eastern Mediterranean atmosphere. Atmos. Environ. **36**, 929–938 (2002)

Krudysz, M.A., Froines, J.R., Fine, P.M., Sioutas, C.: Intra-community spatial variation of size-fractionated PM mass, OC, EC, and trace elements in the Long Beach, CA area. Atmos. Environ. **42**, 5374–5389 (2008)

Li, W.J., Shao, L.Y.: Observation of nitrate coatings on atmospheric mineral dust particles. Atmos. Chem. Phys. **9**, 1863–1871 (2009)

Li, J., Wang, X., Chen, J., Zhu, C., Li, W., Li, C., Liu, C., Xu, C., Wen, L., Xue, L., Wang, W., Ding, A., Herrmann, H.: Chemical composition and droplet size distribution of cloud at the summit of mount tai, China. Atmos. Chem. Phys. **17**, 9885–9896 (2017)

Liao, C.M., Chio, C.P., Chen, W.Y., Ju, Y.R., Li, W.H., Cheng, Y.H., Liao, V.H.C., Chen, S.C., Ling, M.P.: Lung cancer risk in relation to traffic-related nano/ultrafine particle-bound PAHs exposure: a preliminary probabilistic assessment. J. Hazard. Mater. **190**, 150–158 (2011)

Mader, B.T., Schauer, J.J., Seinfeld, J.H., Flagan, R.C., Yu, J.Z., Yang, H., Lim, H.J., Turpin, B.J., Deminter, J.T., Heidemann, G., Bae, M.S., Quinn, P., Bates, T., Eatough, D.J., Huebert, B.J., Bertram, T., Howell, S.: Sampling methods used for the collection of particle-phase organic and elemental carbon during ACE-Asia. Atmos. Environ. **37**, 1435–1449 (2003)

Maji, S., Ahmed, S., Siddiqui, W.A., Ghosh, S.: Short term effects of criteria air pollutants on daily mortality in Delhi, India. Atmos. Environ. **150**, 210–219 (2017)

Mandalakis, M., Apostolaki, M., Tziaras, T., Polymenakou, P., Stephanou, E.G.: Free and combined amino acids in marine background atmospheric aerosols over the eastern Mediterranean. Atmos. Environ. **45**, 1003–1009 (2011)

O'Dowd, C.D., Facchini, M.C., Cavalli, F., Ceburnis, D., Mircea, M., Decesari, S., Fuzzi, S., Yoon, Y.J., Putaud, J.P.: Biogenically driven organic contribution to marine aerosol. Nat. **431**, 676–680 (2004)

Park, S.S., Sim, S.Y., Bae, M.S., Schauer, J.J.: Size distribution of water-soluble components in particulate matter emitted from biomass burning. Atmos. Environ. **73**, 62–72 (2013)

Plaza, J., Pujadas, M., Gómez-Moreno, F.J., Sánchez, M., Artíñano, B.: Mass size distributions of soluble sulfate, nitrate and ammonium in the Madrid urban aerosol. Atmos. Environment. **45**, 4966–4976 (2011)

Rogge, W.F., Hildemann, L.M., Mazurek, M.A., Cass, G.R., Simoneit, B.R.T.: Sources of Fine organic aerosol. 8. Boilers burning no. 2 distillate fuel oil. Environ. Sci. Technol. **31**, 2731–2737 (1997)

Ruddick, K., Neukermans, G., Vanhellemont, Q., Jolivet, D.: Challenges and opportunities for geostationary ocean colour remote sensing of regional seas: a review of recent results. Remote Sens. Environ. **146**, 63–76 (2014)

Sahani, M., Zainon, N.A., Wan Mahiyuddin, W.R., Latif, M.T., Hod, R., Khan, M.F., Tahir, N.M., Chan, C.C.: A case-crossover analysis of forest fire haze events and mortality in Malaysia. Atmos. Environ. **96**, 257–265 (2014)

Salma, I., Füri, P., Németh, Z., Balásházy, I., Hofmann, W., Farkas, Á.: Lung burden and deposition distribution of inhaled atmospheric urban ultrafine particles as the first step in their health risk assessment. Atmos. Environ. **104**, 39–49 (2015)

Shim, C., Lee, J., Wang, Y.: Effect of continental sources and sinks on the seasonal and latitudinal gradient of atmospheric carbon dioxide over East Asia. Atmos. Environ. **79**, 853–860 (2013)

Simoneit, B.R.T., Kobayashi, M., Mochida, M., Kawamura, K., Huebert, B.J.: Aerosol particles collected on aircraft flights over the northwestern Pacific region during the ACE-Asia campaign: composition and major sources of the organic compounds. *J. Geophys. Res. Atmos.* **109**, D19S09 (2004)

Stone, E.A., Yoon, S.C., Schauer, J.J.: Chemical characterization of fine and coarse particles in Gosan, Korea during springtime dust events. Aerosol Air Qual. Res. **11**, 31–43 (2011)

Sullivan, R.C., Moore, M.J.K., Petters, M.D., Kreidenweis, S.M., Roberts, G.C., Prather, K.A.: Timescale for hygroscopic conversion of calcite mineral particles through heterogeneous reaction with nitric acid. Phys. Chem. Chem. Phys. **11**, 7826–7837 (2009)

Tan, J., Duan, J., Zhen, N., He, K., Hao, J.: Chemical characteristics and source of size-fractionated atmospheric particle in haze episode in Beijing. Atmos. Res. **167**, 24–33 (2016)

Tang, G., Zhao, P., Wang, Y., Gao, W., Cheng, M., Xin, J., Li, X., Wang, Y.: Mortality and air pollution in Beijing: the long-term relationship. Atmos. Environ. **150**, 238–243 (2017)

Tyagi, P., Ishimura, Y., Kawamura, K.: Hydroxy fatty acids in marine aerosols as microbial tracers: 4-year study on β- and ω-hydroxy fatty acids from remote Chichijima Island in the western North Pacific. Atmos. Environ. **115**, 89–100 (2015)

Wang, Y.F., Tsai, P.J., Chen, C.W., Chen, D.R., Dai, Y.T.: Size distributions and exposure concentrations of nanoparticles associated with the emissions of oil mists from fastener manufacturing processes. J. Hazard. Mater. **198**, 182–187 (2011)

Wu, Y., Wang, X., Tao, J., Huang, R., Tian, P., Cao, J., Zhang, L., Ho, K.F., Zhang, R.: Size distribution and source of black carbon aerosol in urban Beijing during winter haze episodes. Atmos. Chem. Phys. **17**, 7965–7975 (2017)

Xu, J.Z., Zhang, Q., Wang, Z.B., Yu, G.M., Ge, X.L., Qin, X.: Chemical composition and size distribution of summertime PM2.5 at a high altitude remote location in the northeast of the Qinghai–Xizang (Tibet) plateau: insights into aerosol sources and processing in free troposphere. Atmos. Chem. Phys. **15**, 5069–5081 (2015)

Xu, J., Shi, J., Zhang, Q., Ge, X., Canonaco, F., Prévôt, A.S.H., Vonwiller, M., Szidat, S., Ge, J., Ma, J., An, Y., Kang, S., Qin, D.: Wintertime organic and inorganic aerosols in Lanzhou, China: sources, processes, and comparison with the results during summer. Atmos. Chem. Phys. **16**, 14937–14957 (2016)

Yeatman, S.G., Spokes, L.J., Jickells, T.D.: Comparisons of coarse-mode aerosol nitrate and ammonium at two polluted coastal sites. Atmos. Environ. **35**, 1321–1335 (2001)

Zhang, X., McMurry, P.H.: Evaporative losses of fine particulate nitrates during sampling. Atmos. Environ. **26**, 3305–3312 (1992)

Zhang, Q., Jimenez, J.L., Worsnop, D.R., Canagaratna, M.: A case study of urban particle acidity and its influence on secondary organic aerosol. Environ. Sci. Technol. **41**, 3213–3219 (2007)

Zhao, H., Stephens, B.: Using portable particle sizing instrumentation to rapidly measure the penetration of fine and ultrafine particles in unoccupied residences. Indoor Air. **27**, 218–229 (2017)